Anaylses of Crack Growth in Ductile Solids

A. NEEDLEMAN* and V. TVERGAARD**
*Division of Engineering, Brown University, Providence, RI 02912, USA
**Department of Solid Mechanics, The Technical University of Denmark, Lyngby, Denmark

ABSTRACT

Analyses of ductile crack growth are discussed where the material's constitutive description allows for the possibility of a complete loss of stress carrying capacity, with the associated creation of new free surface. No additional failure criterion is employed so that fracture arises as a natural outcome of the deformation process. Attention is confined to circumstances where the microscale fracture mechanism is ductile void growth. The overall aim is the prediction of parameters characterizing macroscopic toughness, e.g. J_{Ic} and the tearing modulus, in terms of properties describing the fracture mechanism operating on the microscale, e.g. the density and spacing of void nucleating particles. Representative results are presented and some of the numerical challenges raised by this sort of analysis are discussed.

KEYWORDS

Crack growth; ductile fracture; finite element analysis.

INTRODUCTION

Experimental studies of ductile fracture have shown the central role played by microvoid growth in metals (Puttick, 1960, Rogers, 1960, Gurland and Plateau, 1963). The voids nucleate mainly at second phase particles by decohesion of the particle-matrix interface or by particle fracture, and final rupture involves the growth of neighboring voids to coalescence. Analyses of the influence of microscopic voids on plastic flow have been based on a constitutive formulation for progressively cavitating solids (Gurson, 1977). The voids are represented in terms of a single parameter, the void volume fraction, and give rise to dilatancy and pressure sensitivity of the macroscopic plastic deformations. Since the material's constitutive description allows for the possibility of a complete loss of stress carrying capacity with the associated creation of new free surface, fracture arises as a natural outcome of the deformation process. This contrasts with the usual approach to fracture analysis where the constitutive characterization of the material and a fracture criterion are specified separately.

Attention is focussed on circumstances where the fracture mechanism involves two populations of void nucleating particles; larger particles that nucleate voids at relatively small strains and smaller particles that nucleate voids at much larger strains. The spacing between the larger void nucleating particles can serve as a characteristic length. Including a characteristic length into

the boundary value problem formulation is important since macroscopic measures of resistance to crack initiation and growth, e.g. J_{Ic} and the critical crack tip opening displacement, involve linear dimensions (Rice and Johnson, 1970). Therefore, since the constitutive relation does not contain a material length scale, a characteristic length must enter the boundary value problem formulation.

One aim of the analyses discussed here is to relate phenomenological measures of ductility and fracture toughness to measurable (and controllable) features of the material's microstructure. Another aim is to assess the range of applicability of various phenomenological ductile fracture criteria and to provide a method of failure analysis when such criteria cannot be applied.

MATERIAL MODEL

Based on an approximate analysis of a single spherical void, a yield function of the form $\phi(\boldsymbol{\sigma}, \bar{\sigma}, f) = 0$ was proposed (Gurson, 1977) for a porous plastic solid with a randomly distributed volume fraction, f, of voids. Here, $\boldsymbol{\sigma}$ is the macroscopic Cauchy stress tensor and $\bar{\sigma}$ is the matrix flow strength. The flow potential has the form

$$\Phi = \frac{\sigma_e^2}{\bar{\sigma}^2} + 2q_1 f^* \cosh\left(\frac{3q_2\sigma_m}{2\bar{\sigma}}\right) - 1 - q_1{}^2 f^{*2} = 0 \tag{1}$$

where the mean stress, σ_m, and the effective stress, σ_e, are defined in terms of the macroscopic Cauchy stress, $\boldsymbol{\sigma}$, as $\sigma_m = \frac{1}{3}\boldsymbol{\sigma} : \mathbf{I}$ and $\sigma_e^2 = \frac{3}{2}\boldsymbol{\sigma}' : \boldsymbol{\sigma}'$. The stress deviator is given by $\boldsymbol{\sigma}' = \boldsymbol{\sigma} - \mathbf{I}\,\sigma_m$, where $\mathbf{I}$ is the second order identity tensor and $\mathbf{A} : \mathbf{B} = A^{ij}B_{ji}$.

The parameters q_1 and q_2 were introduced to bring predictions of the model at low void volume fractions into closer agreement with full numerical analyses for periodic arrays of voids (Tvergaard, 1981,1982). The function $f^*(f)$ was proposed to represent the more rapid loss of stress carrying capacity associated with void coalescence (Tvergaard and Needleman, 1984). This function is,

$$f^* = \begin{cases} f & f \le f_c\ ; \\ f_c + (f_u^* - f_c)(f - f_c)/(f_f - f_c) & f > f_c \end{cases} \tag{2}$$

so that the modification becomes active when f exceeds a certain critical value, f_c, and the material stress carrying capacity is completely lost for $f = f_f$ (i.e., $f^*(f_f) = f_u^* = 1/q_1$). It is noted that for $q_1 = q_2 = 1$ and $f^* = f$, the function (1) is identical to that originally proposed (Gurson, 1977).

Using (1) as a plastic potential, the flow rule is written as

$$\mathbf{d}^p = \dot{\Lambda}\,\frac{\partial \Phi}{\partial \boldsymbol{\sigma}} \tag{3}$$

The proportionality factor $\dot{\Lambda}$ is determined from the equivalence of the macroscopic dissipation and the dissipation of the matrix material, $\boldsymbol{\sigma} : \mathbf{d}^p = (1 - f)\,\bar{\sigma}\,\dot{\bar{\epsilon}}$, which gives

$$\dot{\Lambda} = [(1 - f)\,\bar{\sigma}\dot{\bar{\epsilon}}]/[\boldsymbol{\sigma} : \frac{\partial \Phi}{\partial \boldsymbol{\sigma}}] \tag{4}$$

The rate of increase of the void volume fraction is taken to be

$$\dot{f} = (1 - f)\,\mathbf{d}^p : \mathbf{I} + \dot{f}_{nucleation} \tag{5}$$

where the first term comes from growth of existing voids with deformation. Two void nucleation criteria have been used; one is a plastic strain criterion for which

$$\dot{f}_{nucleation} = \mathcal{D}\dot{\bar{\epsilon}} \tag{6}$$

while the other is the stress based criterion

$$\dot{f}_{nucleation} = \mathcal{B}(\dot{\sigma}_e + \dot{\sigma}_m) \tag{7}$$

In (6), $\mathcal{D}$ is considered a function of $\bar{\epsilon}$, while analogously in (7), $\mathcal{B}$ is taken to be a function of $(\sigma_e + \sigma_m)$ so that the quantity $(\sigma_e + \sigma_m)$ plays the role of a nucleation stress. In the analyses reviewed here, $\mathcal{D}$ and $\mathcal{B}$ have been specified in terms of a normal distribution about some mean nucleation strain or stress, respectively (Chu and Needleman, 1980). For strain nucleation, $\mathcal{D}$ is written as

$$\mathcal{D} = \frac{f_N}{s_N\sqrt{2\pi}} \exp\left[-\frac{1}{2}\left[\frac{\bar{\epsilon} - \epsilon_N}{s_N}\right]^2\right] \tag{8}$$

where f_N is the volume fraction of void nucleating particles, ϵ_N is the mean strain for nucleation, and s_N is the corresponding standard deviation. For stress nucleation, a similar expression is employed to give a normal distribution about a mean nucleation stress, σ_N.

The matrix plastic strain rate, $\dot{\bar{\epsilon}}$, is specified as

$$\dot{\bar{\epsilon}} = \dot{\epsilon}_0[\bar{\sigma}/g(\bar{\epsilon})]^{1/m}\ ,\ g(\bar{\epsilon}) = \sigma_0(\bar{\epsilon}/\epsilon_0 + 1)^N\ ,\ \epsilon_0 = \sigma_0/E \tag{9}$$

Here, $\bar{\epsilon} = \int \dot{\bar{\epsilon}}dt$ and the function $g(\bar{\epsilon})$ represents the effective stress versus effective strain response in a tensile test carried out at a strain-rate such that $\dot{\bar{\epsilon}} = \dot{\epsilon}_0$. Also, σ_0 is a reference strength and N and m are the strain hardening exponent and strain rate hardening exponent, respectively.

The specification of the constitutive relation is completed by writing the total rate of deformation tensor as the sum of elastic and plastic parts,

$$\mathbf{d} = \mathbf{d}^e + \mathbf{d}^p \tag{10}$$

where the elastic part is expressed in terms of the Jaumann rate of Cauchy stress, $\hat{\boldsymbol{\sigma}}$, by

$$\mathbf{d}^e = \frac{1 + \nu}{E}\hat{\boldsymbol{\sigma}} - \frac{\nu}{E}\,(\hat{\boldsymbol{\sigma}} : \mathbf{I})\,\mathbf{I} = \mathbf{C}^{-1} : \hat{\boldsymbol{\sigma}} \tag{11}$$

Inverting and combining with (3) and (10) gives the stress rate as

$$\hat{\boldsymbol{\sigma}} = \mathbf{C} : \mathbf{d} - \dot{\Lambda}\,\mathbf{C} : \frac{\partial \Phi}{\partial \boldsymbol{\sigma}} \tag{12}$$

FINITE ELEMENT FORMULATION

The incremental constitutive relations are implemented in a Lagrangian convected coordinate finite element formulation that takes full account of finite strains and rotations, e.g. (Needleman, 1982). Attention is confined to quasi-static deformations and expansion of the principle of virtual work about a known reference state gives,

$$\Delta t \int_V \dot{\mathbf{n}} : (\nabla \delta\mathbf{u})\,dV = \Delta t \int_S \dot{\mathbf{T}} \cdot \delta\mathbf{u}\,dS - \left[\int_V \mathbf{n} : (\nabla\delta\mathbf{u})\,dV - \int_S \mathbf{T} \cdot \delta\mathbf{u}\,dS\right] \tag{13}$$

Here, $\mathbf{n} = J\,\mathbf{F}^{-1} \cdot \boldsymbol{\sigma}$ is the nominal stress where $\mathbf{F} = \mathbf{I} + \nabla\mathbf{u}$ is the deformation gradient and $J = \det(\mathbf{F})$ is the Jacobian of the deformation. The surface traction vector is denoted by $\mathbf{T}$ and ∇ is the material gradient operating on the displacement, $\mathbf{u}$. Spatial integrations are carried out over the reference volume, V, and surface, S. The bracketed term on the right hand side is an equilibrium correction term to adjust for any slight out of balance forces arising from finite time steps. For the range of strain rate sensitivity considered in these analyses, the equations

are numerically "stiff" and require small time steps for stable numerical integration. A rate tangent modulus method (Pierce *et al.*, 1984) is employed to increase the stable time step size.

The finite element mesh consists of quadrilaterals built up of "crossed" linear displacement triangular elements. Such a grid is suited for isochoric deformations (Nagtegaal, Parks and Rice, 1974) which is important since relatively large plastic strains can occur prior to void nucleation. However, the primary motivation for choosing this type of mesh stems from the need to resolve narrow shear bands. A suitably oriented "crossed" triangle mesh can resolve narrow localization bands; if the orientation is not optimal or if a finite element mesh consisting of ordinary isoparametric elements is used, localization can be obtained numerically, but with some delay and with a mesh induced shear band broadening (Tvergaard *et al.*, 1981). An alternative to the "crossed" triangle arrangement is a recently proposed enhanced element method (Ortiz, Leroy and Needleman, 1987).

DUCTILE FRACTURE AT A CRACK TIP

Calculations of critical conditions for crack initiation by analysis of void growth and coalescence in crack tip fields initiated in (Rice and Johnson, 1970, McMeeking, 1977). Subsequently, the coupling of progressive fracture events with the surrounding field was considered through finite element analyses of plane strain tensile cracks under small scale yielding conditions (Aoki *et al.*, 1984, Aravas and McMeeking, 1985ab, Needleman and Tvergaard, 1987). The interaction of a single void with the crack tip has been considered (Aoki *et al.*, 1984, Aravas and McMeeking, 1985ab), while the nucleation of larger voids from "islands" of increased density of the amplitude of the void nucleation function was analyzed in (Needleman and Tvergaard, 1987). The latter formulation (Needleman and Tvergaard, 1987) has the advantage of representing a material with no voids in the initial state, so that the full effect of the near tip stress and strain fields on nucleation and growth is described. Furthermore, with the inclusions represented as islands of increased nucleation amplitude, it is feasible to study the effect of an array of larger inclusions, interacting with the crack tip and with one another.

Here, we present some results for a full specimen, a center cracked panel. As in a previous study (Needleman and Tvergaard, 1987), the distribution of small scale particles is taken to be uniform and nucleation at these particles is taken to be governed by the strain controlled criterion, (8), with $f_N = 0.02$, $\epsilon_N = 0.3$ and $s_N = 0.1$. Nucleation at the larger particles is taken to be stress controlled with $f_N = 0.04$, $\sigma_N = 2.2\sigma_0$ and $s_N = 0.1\sigma_0$, and their spatial distribution is modelled by a square array of "islands" of increased density of the amplitude of the void nucleation function. The matrix material properties are given by $N = 0.1$, $m = 0.01$ and $\epsilon_0 = 0.002$ in (9). The center cracked panel dimensions are height (specimen length perpendicular to the crack line) $2h$, width (specimen width parallel to the crack line) $2w$, and crack length $2a$ where in the calculation reported on here $a/w = 0.5$ and $h/w = 2.0$ and one quarter of the specimen is analyzed numerically. The crack is represented by an initially semi-circular notch of radius $2 \times 10^{-4}w$. The distance between "islands" is $2 \times 10^{-3}w$ and their radius is the same as that of the semi-circular notch, $2 \times 10^{-4}w$.

Figure 1 shows the load versus overall strain curve for the center cracked panel. Here, the load is normalized by the limit load for a perfectly plastic solid having yield stress σ_0, $4\sigma_0(w-a)/\sqrt{3}$, and the overall strain, U/h, is normalized by ϵ_0. For the case analyzed here, the onset of crack growth occurs very near the limit load. Figure 2 shows contours of accumulated matrix plastic strain, $\bar{\epsilon}$, prior to (Fig. 2a) and during crack growth (Figs. 2b and 2c). Plastic straining mainly occurs in a 45° band emanating from the crack tip. The stages of deformation are characterized by the value of the J-integral (Rice, 1968) as well as by the applied load.

The assumption that the larger inclusions have relatively low strength, while the smaller particles require large straining prior to nucleation, has a significant influence on the fracture mechanism. Self-similar stress and strain fields develop during crack tip blunting and sweep

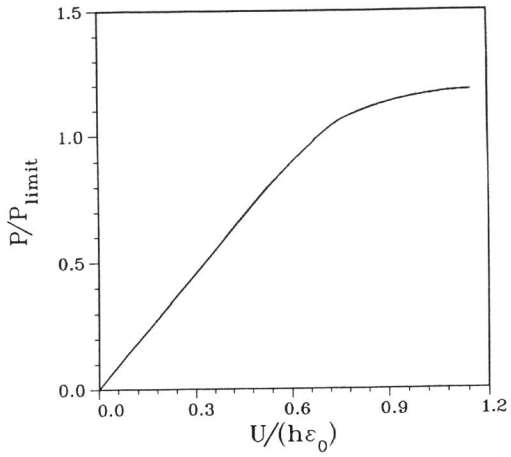

Fig. 1. Load versus overall strain for a center cracked panel with $a/w = 0.5$.

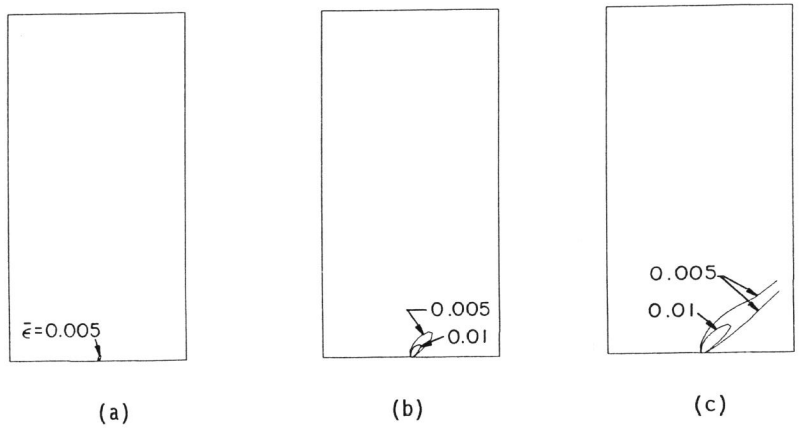

Fig. 2. Contours of constant matrix effective plastic strain, $\bar{\epsilon}$, in the quadrant analyzed numerically at (a) $P/P_{limit} = 0.80$, $(w-a)\sigma_0/\mathrm{J} = 550$ (b) $P/P_{limit} = 1.12$, $(w-a)\sigma_0/\mathrm{J} = 175$ and (c) $P/P_{limit} = 1.18$, $(w-a)\sigma_0/\mathrm{J} = 99$.

over the near tip material, so that a particle at initial distance R is reached by the stress peak when $\mathrm{J}/\sigma_0\mathrm{R} \approx 0.5$, while the strains are still very small (Rice and Johnson, 1970, McMeeking, 1977). After a void has nucleated, it is engulfed by the field of large strains so that it starts to grow, while small scale voids nucleate in the ligament between the crack tip and the larger void. The process repeats itself when inclusions that were initially further away from the crack tip are reached by the stress peak. This mechanism of crack growth is illustrated in Fig. 3, where near tip contours of effective stress show crack growth through subsequent nucleation of seven larger

voids. In Fig. 3a, the matrix flow strength contours reflect the presence of the "islands" of the void nucleation function amplitude representing the large particles. The $\bar{\sigma}/\sigma_0 = 1.4$ contour is of the shape expected from the HRR field (Hutchinson, 1968, Rice and Rosengren, 1968). The effect of the overall center cracked panel deformation pattern is seen in the other contours. The transition to crack growth type fields (Drugan *et. al*, 1982) is evident in Figs. 3b and 3c. In particular, note the unloading wedge behind the propagating crack tip.

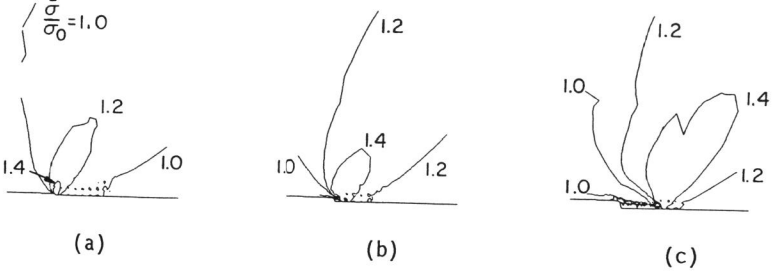

Fig. 3. Contours of matrix flow strength, $\bar{\sigma}/\sigma_0$, near the crack tip at (a) $P/P_{limit} = 0.80$, $(w-a)\sigma_0/J = 550$ (b) $P/P_{limit} = 1.12$, $(w-a)\sigma_0/J = 175$ and (c) $P/P_{limit} = 1.18$, $(w-a)\sigma_0/J = 99$.

One feature associated with this sort of calculation is the large stress redistribution that occurs as the crack grows. This is illustrated in Fig. 4, which shows contours of hydrostatic stress at these three stages of crack growth. As the crack grows, the hydrostatic stress peak moves.

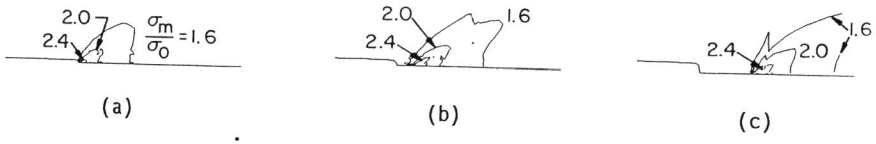

Fig. 4. Contours of normalized mean normal stress, σ_m/σ_0, near the crack tip at (a) $P/P_{limit} = 0.80$, $(w-a)\sigma_0/J = 550$ (b) $P/P_{limit} = 1.12$, $(w-a)\sigma_0/J = 175$ and (c) $P/P_{limit} = 1.18$, $(w-a)\sigma_0/J = 99$.

Localized shearing in the form of a void sheet plays a role in the fracture process, as illustrated in Fig. 5. The elements painted black have undergone a complete loss of stress carrying capacity and their boundary represents free surface created by the fracture process.

Previous small scale yielding calculations (Needleman and Tvergaard, 1987) and the full specimen calculation presented here appear to provide accurate descriptions of modes of ductile failure at a crack tip and illustrate the dependence of crack initiation and growth on microstructural features such as the distribution and nucleation characteristics of second phase particles. These calculations also give quantitative predictions of the dependence of crack initiation and growth on microstructural features. Figure 6 depicts predicted dependence of crack initiation on inclusion size and spacing, together with a summary of experimental results. More recently, a similar computational framework has been used in a combined numerical and experimental study of ductile fracture by grain boundary void growth in Al-Li alloys (Becker *et al.*, 1988).

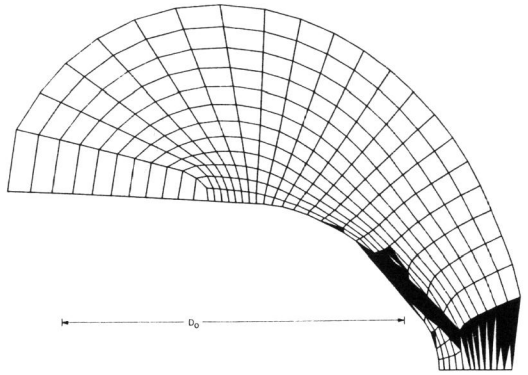

Fig. 5. Deformed near tip finite element mesh. A complete loss of stress carrying capacity has occurred in the elements painted black. From (Needleman and Tvergaard, 1987).

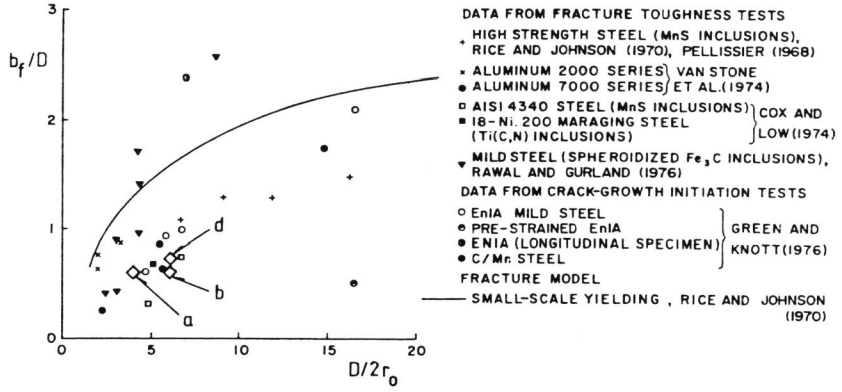

Fig. 6. Crack tip opening b_f at fracture initiation, related to particle spacing D and particle size $2r_0$. Results of previous computations (Needleman and Tvergaard, 1987), indicated by *a*, *b* and *d* are plotted along with summarized experimental data (McMeeking, 1977). Here, *a*, *b* and *d* refer to various distributions of the large particles. From (Needleman and Tvergaard, 1987).

ACKNOWLEDGEMENTS

The support of the Office of Naval Research through grant N0001486-K-0262 is gratefully acknowledged. The computations reported on here were carried out on the supercomputer facilities of the Naval Research Laboratory.

Aoki, S., K. Kishimoto, A. Takeya and M. Sakata (1984). Effects of microvoids on crack tip blunting and initiation in ductile materials. *Int. J. Frac.*, **28**, 267-278.

Aravas, N. and R.M. McMeeking (1985a). Finite element analysis of void growth near a blunting crack tip. *J. Mech. Phys. Solids*, **33**, 25-49.

Aravas, N. and R.M. McMeeking (1985b). Microvoid growth and failure in the ligament between a hole and a blunt crack tip. *Int. J. Frac.*, **29**, 21-38.

Becker, R., A. Needleman, S. Suresh, V. Tvergaard and A.K. Vasudevan (1988). An analysis of ductile failure by grain boundary void growth. *Acta Metall.*, to be published.

Chu, C.C. and A. Needleman (1980). Void nucleation effects in biaxially stretched sheets. *J. Engng. Mat. Tech.*, **102**, 249-256.

Drugan, W.J., J.R. Rice and T.-L. Sham (1982). Asymptotic analysis of growing plane strain tensile cracks in elastic-ideally plastic solids. *J. Mech. Phys. Solids*, **30**, 447-473.

Gurland, J. and J. Plateau (1963). The mechanism of ductile rupture of metals containing inclusions. *Trans. ASM*, **56**, 442-454.

Gurson, A.L. (1977). Continuum theory of ductile rupture by void nucleation and growth: part I yield criteria and flow rules for porous ductile materials. *J. Engng. Mat. Tech.*, **99**, 2-15.

Hutchinson, J.W. (1968). Singular behavior at the end of a tensile crack in a hardening material. *J. Mech. Phys. Solids*, **16**, 13-31.

McMeeking, R.M. (1977). Finite deformation analysis of crack-tip opening in elastic-plastic materials and implications for fracture. *J. Mech. Phys. Solids*, **25**, 357-381.

Nagtegaal, J.C., D.M. Parks and J.R. Rice (1974). On numerically accurate finite element solutions in the fully plastic range. *Comp. Meth. Appl. Mech. Eng.*, **4**, 153-177.

Needleman, A. (1982). Finite elements for finite strain plasticity problems. In: *Plasticity of Metals at Finite Strain: Theory, Computation and Experiment*, (eds. E. H. Lee and R. L. Mallett), pp. 387-436.

Needleman, A. and V. Tvergaard (1987). An analysis of ductile rupture modes at a crack tip. *J. Mech. Phys. Solids*, **35**, 151-183.

Ortiz, M., Y. Leroy and A. Needleman (1987). A finite element method for localized failure analysis. *Comp. Meth. Appl. Mech. Engr.*, **61**, 189-214.

Pierce, D., C.F. Shih and A. Needleman (1984). A tangent modulus method for rate dependent solids. *Comp. Struct.*, **18**, 875-887.

Puttick, K.E. (1960). Ductile fracture in metals. *Phil. Mag.* Ser. 8, **4**, 964-969.

Rice, J.R., A path independent integral and the approximate analysis of strain concentration by notches and cracks. *J. Appl. Mech.*, **35**, 1968, 379-386.

Rice, J.R. and M.A. Johnson (1970). The role of large crack tip geometry changes in plane strain fracture. In: *Inelastic Behavior of Solids*, (ed. M.F. Kanninen et al.), pp. 641-661.

Rice, J.R. and G.F. Rosengren (1968). Plane strain deformation near a crack tip in a power law hardening material. *J. Mech. Phys. Solids*, **16**, 1-12.

Rogers, H.C. (1960). The tensile fracture of ductile metals. *Trans. TMS-AIME*, **218**, 498-506.

Tvergaard, V. (1981). Influence of voids on shear band instabilities under plane strain conditions. *Int. J. Fract.*, **17**, 389-407.

Tvergaard, V. (1982). On localization in ductile materials containing spherical voids. *Int. J. Fract.*, **18**, 237-252.

Tvergaard, V. and A. Needleman (1984). Analysis of the cup-cone fracture in a round tensile bar. *Acta Metall.*, **32**, 157-169.

Tvergaard, V., A. Needleman and K.K. Lo (1981). Flow localization in the plane strain tensile test. *J. Mech. Phys. Solids*, **29**, 115-142.